Supplement of Atmos. Chem. Phys., 26, 547–570, 2026
https://doi.org/10.5194/acp-26-547-2026-supplement

Atmospheric Chemistry and Physics
Open Access
EGU

Supplement of

Estimation of CO_2 fluxes in the cities of Zurich and Paris using the ICON-ART CTDAS inverse modelling framework

Nikolai Ponomarev et al.

Correspondence to: Nikolai Ponomarev (nikolai.ponomarev@empa.ch) and Dominik Brunner (dominik.brunner@empa.ch)

This supplementary document provides additional details and supporting information for the main text. The first section presents additional maps of emissions and land cover and figures of additional performance statistics and time series analyses. The second section presents additional tables describing the stations used in the inversions in Zurich and Paris as well as anthropogenic and biospheric flux estimates separately for summer and winter.

S1 Supplement

S1.1 Figures

Figure S1 shows the annual mean anthropogenic CO_2 emissions over central Europe for 2021. The emission data are based on the TNO-GHGco inventory and are mapped onto the ICON-ART model grid at a spatial resolution of 6.6 km.

Figure S2 illustrates how well the ICON-ART model reproduces observed afternoon (11:00–16:00 UTC) CO_2 mole fractions at ICOS sites across Europe. The sites located within the model domain and used for these comparisons are listed in Table S2.

In order to better represent the vegetation cover in Zurich, we used a high-resolution (10 m) dataset developed within the ICOS cities project. The methodology for creating this dataset is described in Stagakis et al. (2025). Figure S3 demonstrates the results.

Figure S4 compares urban land use fraction estimates used as input to the ICON-ART model in Zurich and Paris. Panel (a) shows the custom high-resolution dataset for Zurich, while panels (b) and (c) show CORINE 2018 data. The comparison highlights significant differences in terms of the total urban area fractions and indicates an underestimation of vegetated areas by CORINE 2018.

In order to evaluate the model performance in terms of meteorology, we compared simulated wind speed and temperature at urban and non-urban sites in Zurich and Paris. Figure S5 shows the results for Zurich at two sites: zhhf (Kantonales Labor Zürich) and klof (Kloten Feld). The overall day-to-day patterns are reproduced well by the model for both temperature and wind speed. However, it tends to underestimate wind speed during nighttime and calm weather conditions.

Comparisons for two sites in Paris, CDS (Cité des Sciences) and SAC (Saclay), are present in Figure S6. Again, the model performs well, capturing the changes in temperature and wind speed. At CDS, it tends to overestimate wind speeds, likely due to the fact that buildings are not explicitly represented in the mesoscale model.

In Zurich, we had access to a larger number of meteorological observation sites, allowing for a more detailed evaluation of model performance. Figures S8 and S9 summarize the annual and monthly statistics of temperature and wind speed, respectively. The temperature bias is generally small and positive, around 0.21 K on average. Its largest values occur in summer 2023. The annual bias on most of the sites remains below 0.5 K, except for zhmi (Milchbuck Schule), which shows a larger value. Overall, the temperature is well reproduced by the model, with a high correlation of 0.92 compared to observations.

For wind speed, the bias was negative during the September–December 2022 period, becoming positive for the remainder of the simulations and averaging about 0.27 $m\,s^{-1}$. Most sites show biases in the range of 0.5 and 1 $m\,s^{-1}$, with zhmi (Milchbuck Schule) and zjho (Limmattalstrasse Höngg) showing larger differences. As expected, correlations for wind speed are lower, averaging around 0.64. Finally, in Fig. S7, modeled wind speeds at the rooftop site Kantonales Labor in Zurich are compared to observations for 15 December 2022 to 13 January 2023. The model reproduces day-to-day variability reasonably well when winds exceed 1 $m\,s^{-1}$, but tends to underestimate wind speeds during prolonged calm periods.

To illustrate the separation of flux components achieved by the inversion system, we provide additional figures showing the spatial distributions and diurnal cycles of anthropogenic emissions, GPP, and RE. Figure S10 presents the hourly mean diurnal cycles of these fluxes for Zurich (top) and Paris (bottom), highlighting the contribution of each component throughout the day. Figure S11 shows maps of posterior minus prior flux adjustments for anthropogenic emissions, RE, and GPP, with the top row for Zurich and the bottom row for Paris, emphasizing the spatial patterns of inversion updates. These figures complement the main text by providing a clearer comparison of the three flux components and their temporal and spatial variations.

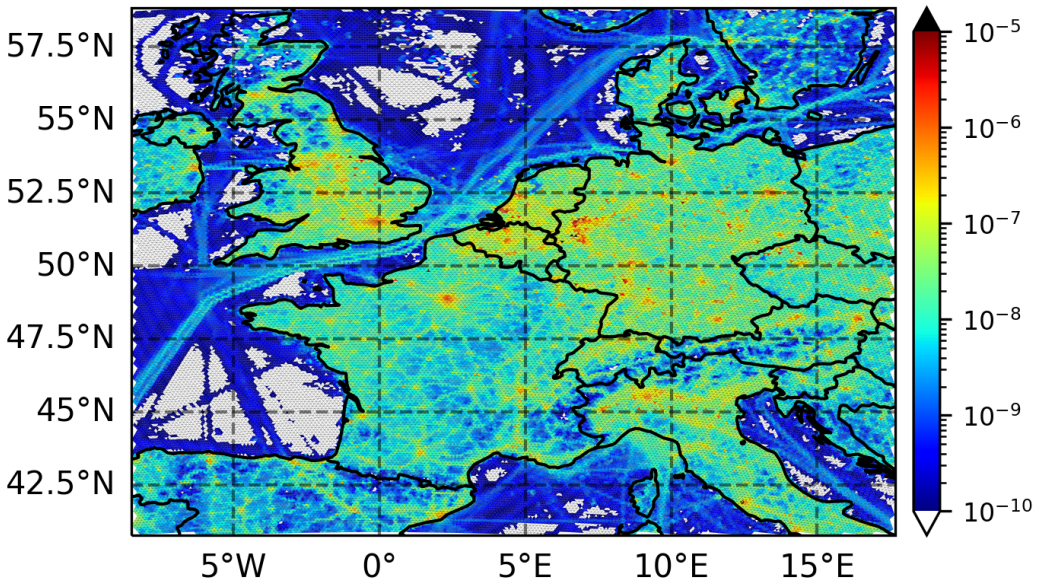

Figure S1. The annual mean anthropogenic CO_2 emissions from the TNO-GHGco inventory for the year 2021 shown on ICON-ART model grid within the domain over central Europe with 6.6 km spatial resolution. The inventory was based on the 2023 official reporting of 2021 emissions (AVENGERS project), except for shipping emissions. Those were taken from the 2021 version of the TNO-GHGco inventory used in the CoCO2 project reflecting an earlier country reporting version for that sector.

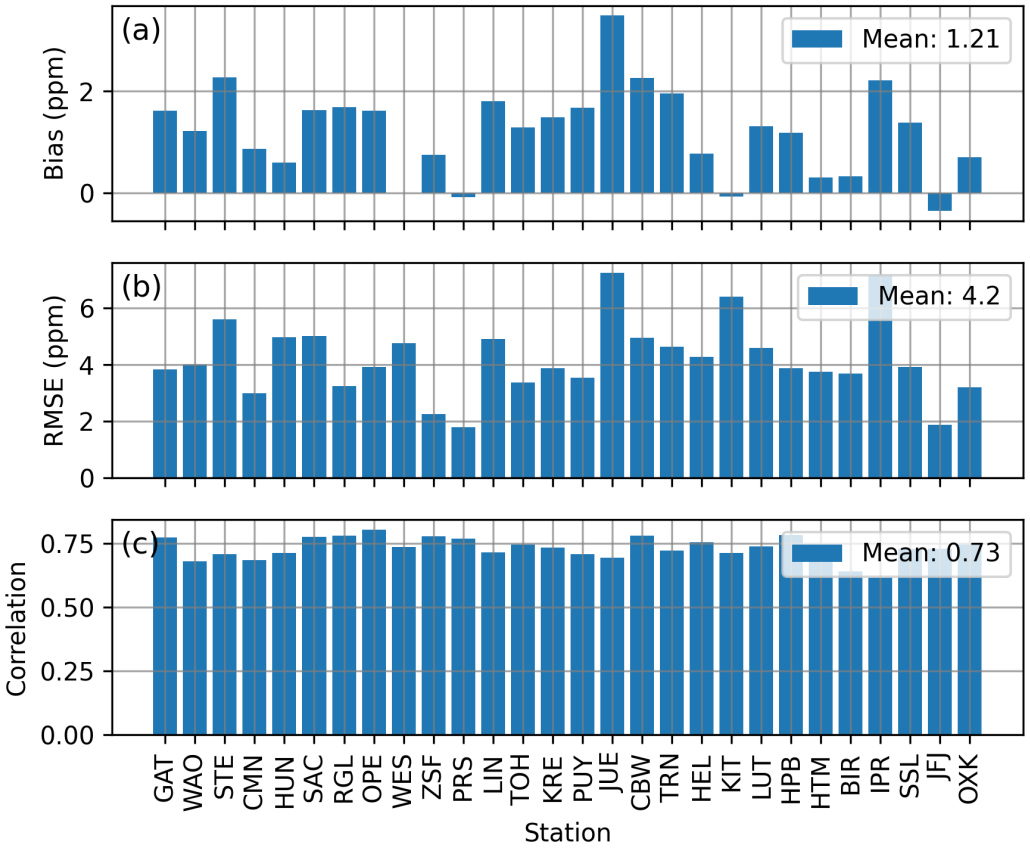

Figure S2. Annual statistics of mean modeled versus observed afternoon CO_2 mole fractions at ICOS stations in the European model domain. Panel (a) shows monthly mean biases for each site inside the model domain, (b) RMSEs, and (c) correlation coefficients.

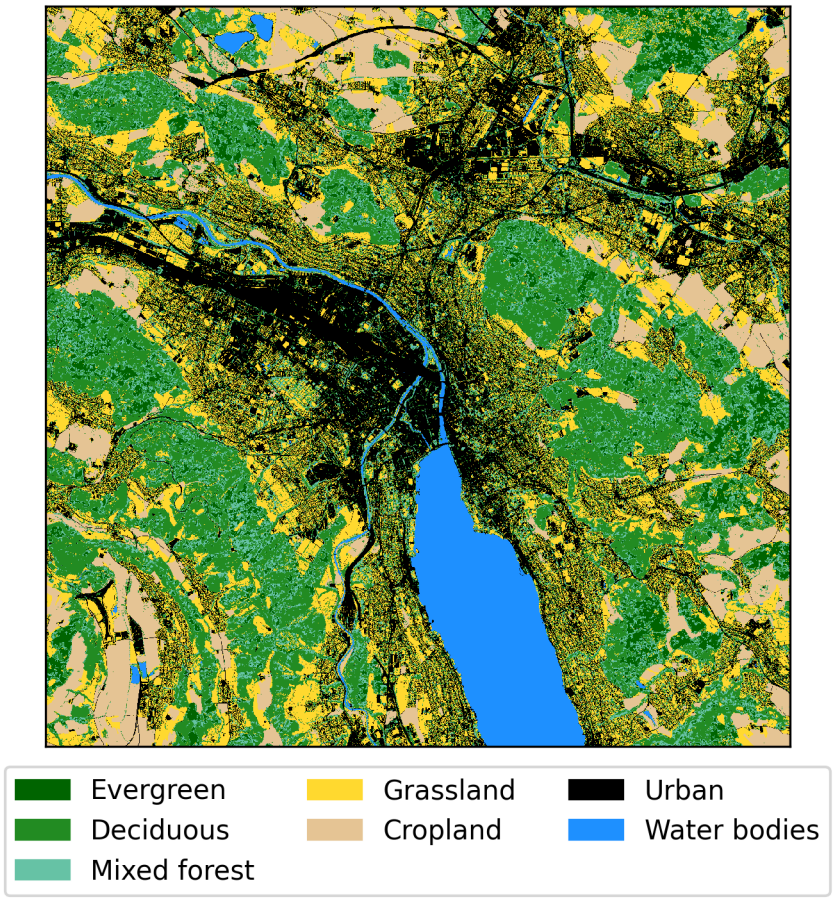

Figure S3. Landuse data in the city of Zurich at 10 m resolution (Stagakis et al., 2025).

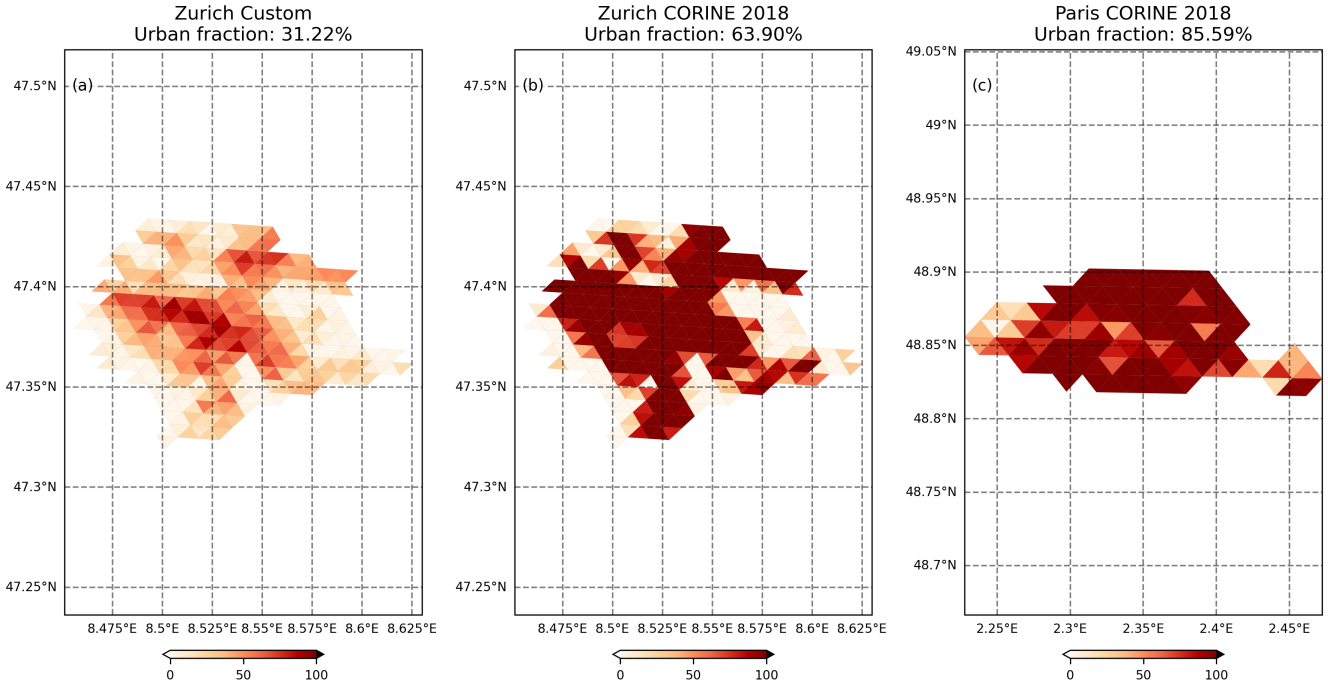

Figure S4. The urban land use fraction in Zurich and Paris, based on a custom made dataset (a) for Zurich and the CORINE 2018 (b), (c).

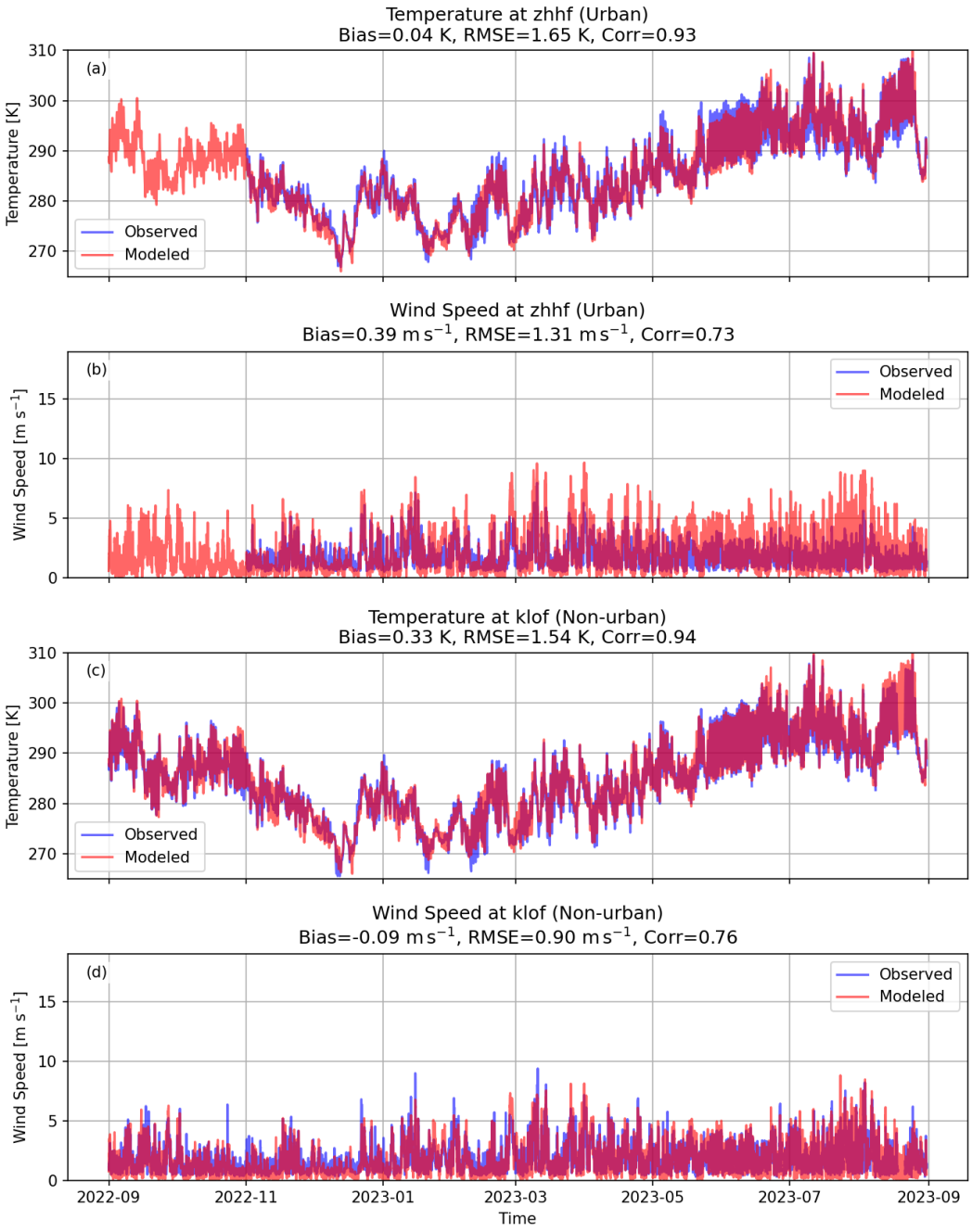

Figure S5. Wind speed and temperature comparison for an urban (a), (b) and non urban (c), (d) sites in Zurich.

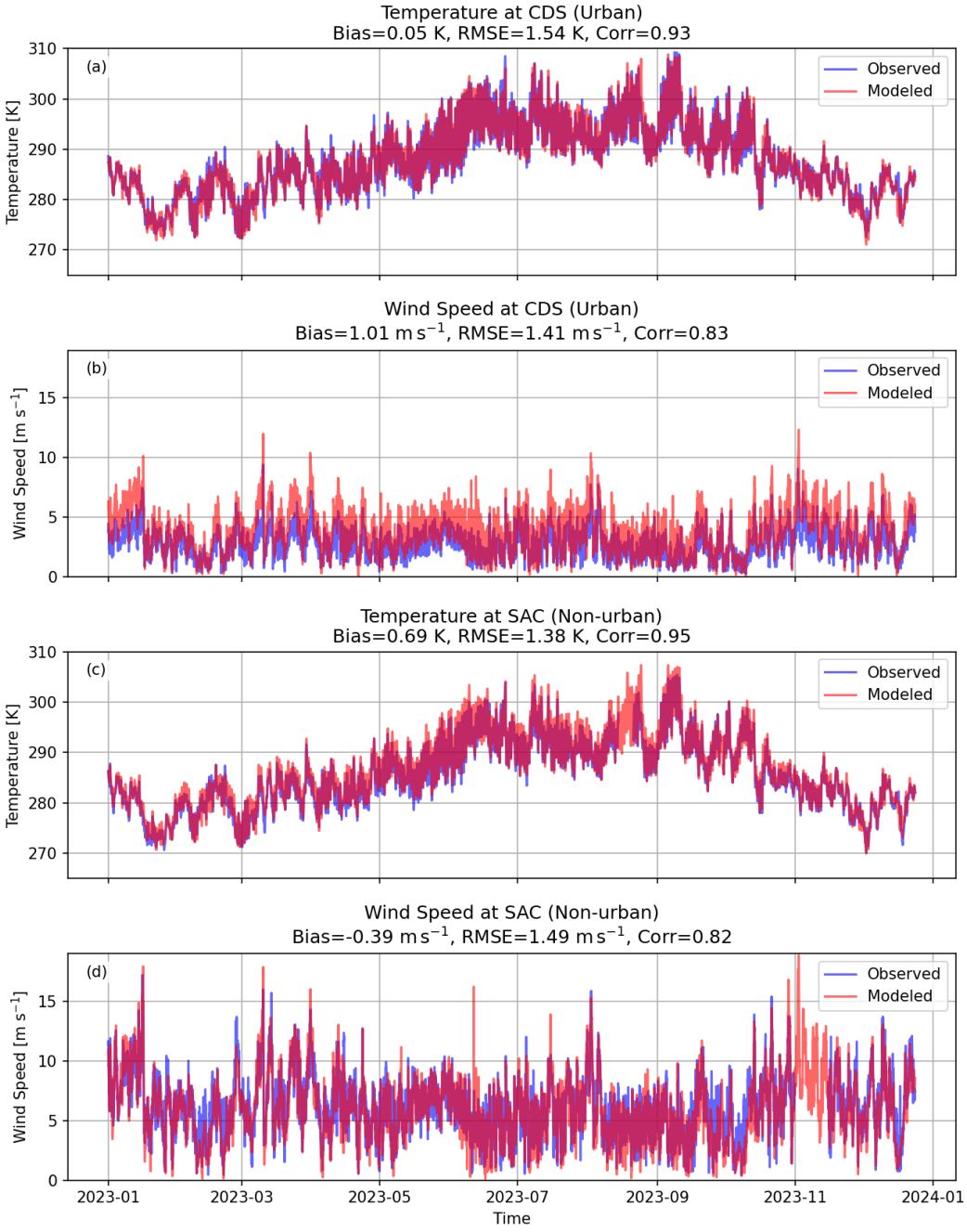

Figure S6. Wind speed and temperature comparison for an urban (a), (b) and non urban (c), (d) sites in Paris.

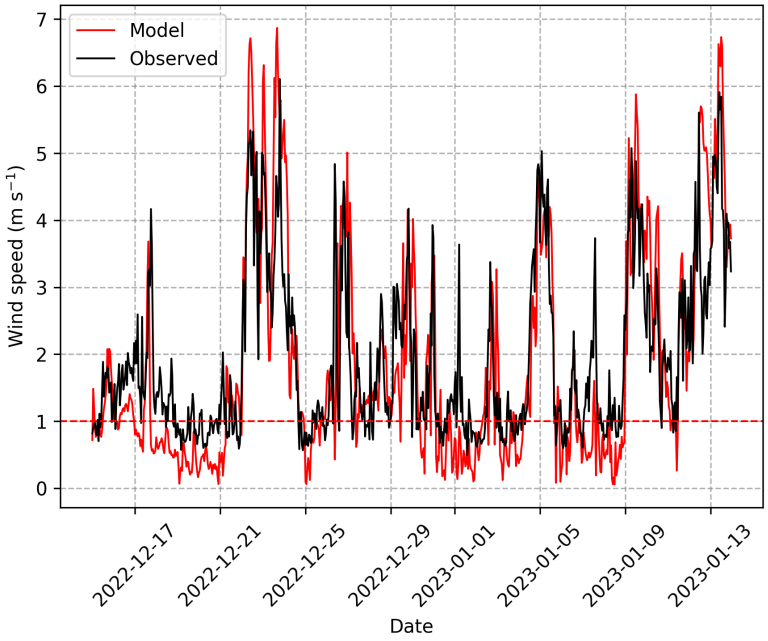

Figure S7. Comparison of modeled and observed wind speed at the rooftop site Kantonales Labor in Zurich for the period 15 December 2022 to 13 January 2023.

S1.2 Tables

Table S1 lists the meteorological observation sites in Zurich used for temperature and wind speed evaluation, sorted by latitude. Table S2 summarizes the European ICOS sites included in this study. Finally, Table S3 presents the prior and posterior fluxes along with their absolute uncertainties and their reductions for Zurich and Paris across flux categories in summer and winter seasons.

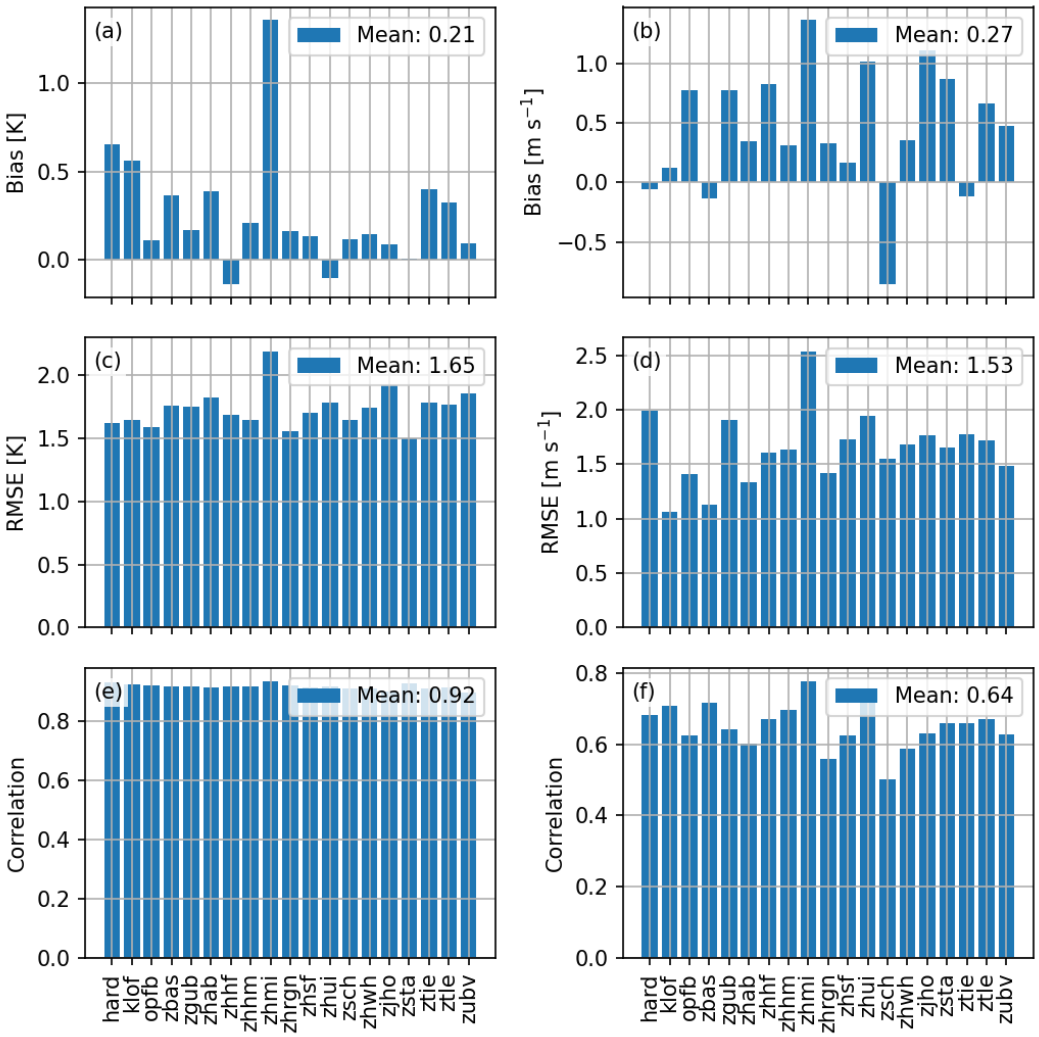

Figure S8. Annual statistics of mean modeled versus observed afternoon wind speed and temperature values in Zurich. Panels (a), (c), (e) show annual mean temperature Bias, RMSE, and correlation, correspondingly, while panels (b), (d), (f) show similar statistics for the wind speed.

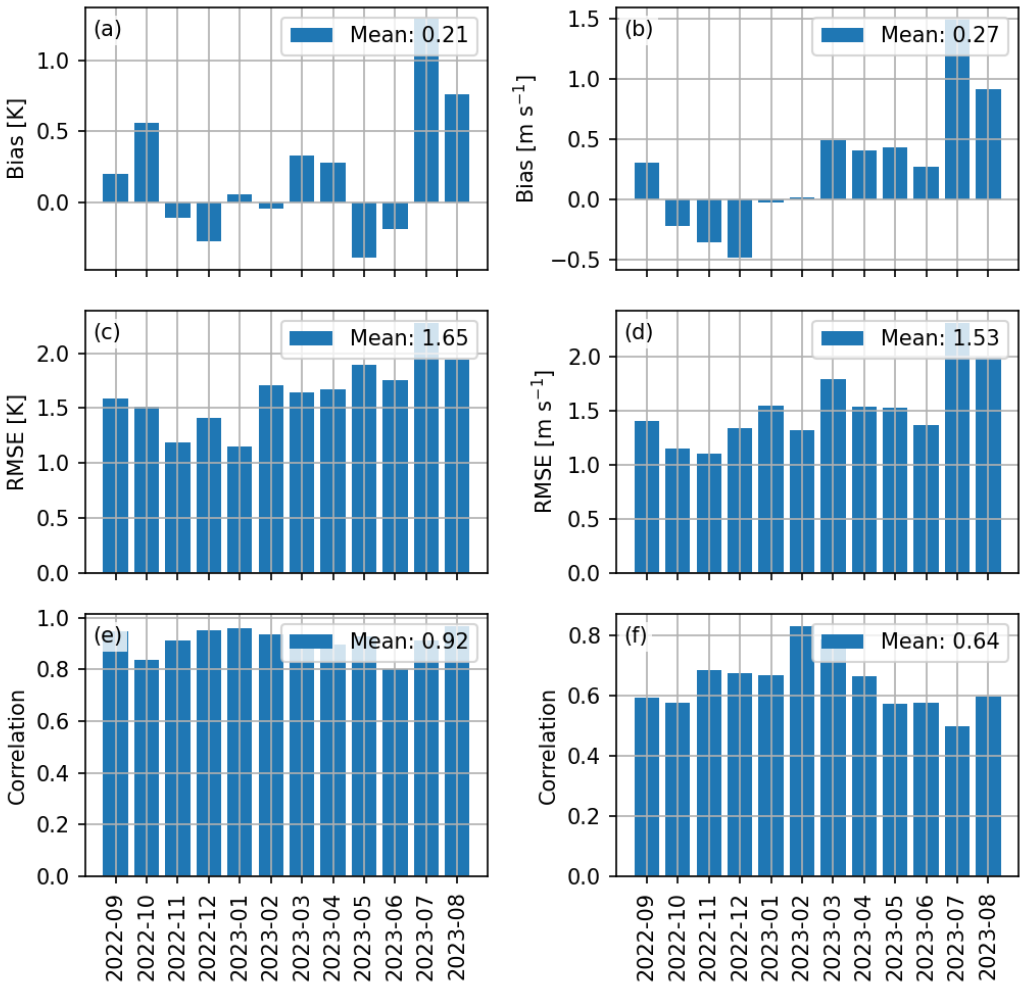

Figure S9. Monthly statistics of averaged across all sites modeled and observed afternoon wind speed and temperature values in Zurich. Panels (a), (c), (e) show annual mean temperature Bias, RMSE, and correlation, correspondingly, while panels (b), (d), (f) show similar statistics for the wind speed.

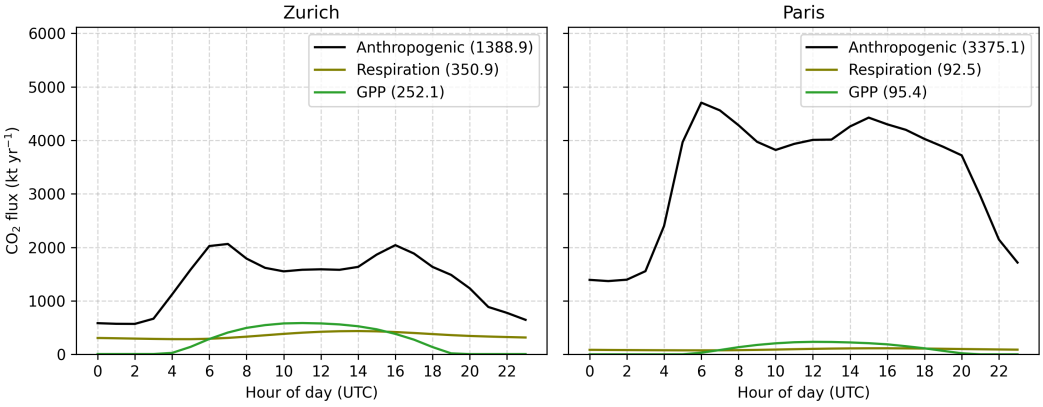

Figure S10. Diurnal cycles of CO_2 anthropogenic emissions, GPP, and RE for Zurich (left) and Paris (right). Mean daily fluxes are indicated in parentheses in the legend.

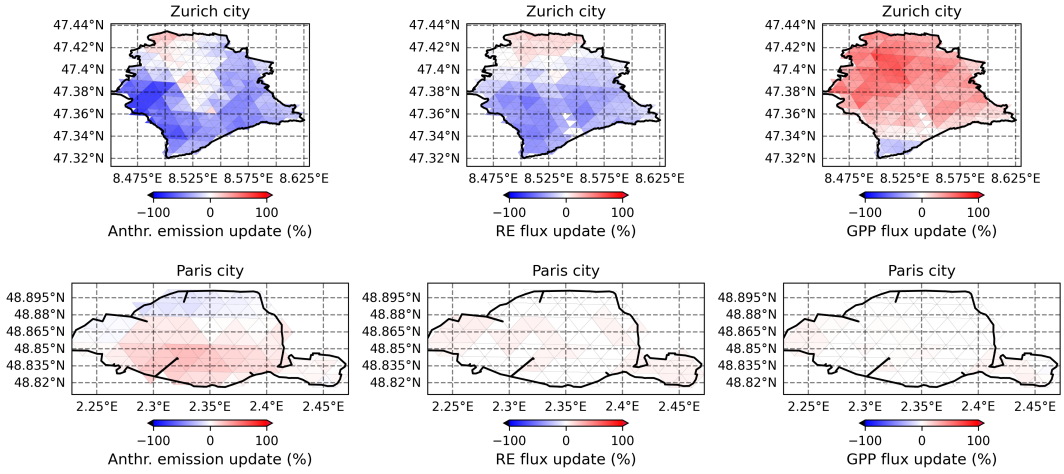

Figure S11. Maps of flux adjustments for anthropogenic emissions, RE, and GPP. Top row: Zurich; bottom row: Paris. Values represent posterior minus prior fluxes, expressed as a percentage of the prior values. For GPP, positive values correspond to stronger biogenic uptake.

Table S1. Sites used for temperature (T) and wind speed (WS) comparison against the model in Zurich, sorted by latitude descending.

Acronym	Name	Longitude	Latitude	Elevation (m)	Inlet height T (m)	Inlet height WS (m)
klof	Kloten Feld	8.5840	47.4548	440.0	4.0	4.0
opfb	Opfikon Balsberg	8.5701	47.4388	430.0	4.0	4.0
zhmi	Schule Milchbuck	8.5378	47.3957	477.7	37.5	37.5
zhrgn	Rosengartenstrasse	8.5261	47.3952	432.7	3.3	4.9
zhui	Universität Zürich Irchel	8.5506	47.3987	491.7	30.5	30.5
zjho	Limmattalstrasse Höngg	8.4881	47.4036	441.4	13.9	13.9
zsta	Stampfenbachstrasse	8.5398	47.3867	420.8	4.5	28.5
zhhm	Hardturmstrasse Förrlibuck	8.5153	47.3920	401.2	41.4	41.4
zbas	Badenerstrasse Farbhof	8.4803	47.3904	399.6	23.3	23.3
hard	Hardau II	8.5101	47.3813	409.4	110.3	110.3
zgub	Güterbahnhof	8.5176	47.3817	407.5	30.2	30.2
ztle	Letzigraben Telefonzentrale	8.5005	47.3787	411.8	25.2	25.2
zhsf	Stauffacherstrasse Werdplatz	8.5288	47.3724	411.4	48.5	48.5
zsch	Schimmelstrasse	8.5236	47.3710	413.1	3.4	5.5
zhhf	Kantonales Labor Zürich	8.5585	47.3713	451.8	21.4	21.4
zubv	Bankenviertel Bleicherweg	8.5380	47.3689	408.7	27.1	27.1
zhab	Albisgüetli	8.5128	47.3535	469.8	23.0	23.0
ztie	Tiefenbrunnen Wildbachstrasse	8.5588	47.3530	408.7	39.4	39.4
zhwh	Wollishofen	8.5333	47.3470	407.9	42.3	42.3

Table S2. European ICOS sites used in this study. All sites are equipped with high-precision instruments. Elevation refers to height above sea level, and inlet height to height above ground level.

Acronym	Name	Longitude	Latitude	Elevation (m)	Inlet height (m)
BIR	Birkenes	8.2519	58.3886	294.0	75.0
HTM	Hyltemossa	13.4189	56.0976	265.0	150.0
WES	Westerland	8.3080	54.9231	26.0	14.0
HEL	Helgoland	7.8833	54.1804	153.0	110.0
LUT	Lutjewad	6.3528	53.4036	61.0	60.0
GAT	Gartow	11.4429	53.0657	411.0	341.0
STE	Steinkimmen	8.4588	53.0431	281.0	252.0
WAO	Weybourne	1.1210	52.9500	27.0	10.0
LIN	Lindenberg	14.1226	52.1663	171.0	98.0
RGL	Ridge Hill	-2.5399	51.9975	297.0	90.0
CBW	Cabauw	4.9264	51.9703	207.0	207.0
TOH	Torfhaus	10.5350	51.8088	948.0	147.0
JUE	Jülich	6.4096	50.9102	218.0	120.0
OXK	Ochsenkopf	11.8083	50.0300	1185.0	163.0
KRE	Křešín u Pacova	15.0800	49.5720	784.0	250.0
KIT	Karlsruhe	8.4249	49.0915	310.0	200.0
SAC	Saclay	2.1420	48.7227	260.0	100.0
OPE	Observatoire pérenne de l'environnement	5.5036	48.5619	510.0	120.0
TRN	Trainou	2.1125	47.9647	311.0	180.0
SSL	Schauinsland	7.9166	47.9167	1240.0	35.0
HPB	Hohenpeissenberg	11.0246	47.8011	1065.0	131.0
ZSF	Zugspitze	10.9796	47.4165	2669.0	3.0
HUN	Hegyhátsál	16.6522	46.9558	363.0	115.0
JFJ	Jungfraujoch	7.9851	46.5475	3585.7	13.9
PRS	Plateau Rosa	7.7000	45.9300	3490.0	10.0
IPR	Ispra	8.6360	45.8147	310.0	100.0
PUY	Puy de Dôme	2.9658	45.7719	1475.0	10.0
CMN	Monte Cimone	10.6999	44.1936	2173.0	8.0

Table S3. Prior and posterior fluxes with absolute uncertainties and their reductions for Zurich and Paris across categories in summer and winter seasons based on the results of this study.

City	Season	Category	Prior flux ± uncertainty (kt/yr)	Posterior flux ± uncertainty (kt/yr)	Absolute uncertainty reduction (kt/yr)	Uncertainty reduction (%)
Zurich	Summer	Total	998.8 ± 242.8	735.9 ± 156.8	86.0	35.4
	Winter	Total	2018.3 ± 431.7	1021.5 ± 47.2	384.5	89.1
	Summer	Anthropogenic	961.9 ± 205.3	1042.7 ± 112.7	92.6	45.1
	Winter	Anthropogenic	1909.6 ± 430.9	928.5 ± 42.3	388.7	90.2
	Summer	NEE	36.9 ± 129.5	-306.8 ± 109.0	20.5	15.9
	Winter	NEE	108.6 ± 26.2	93.0 ± 21.0	5.2	19.8
	Summer	RE	565.8 ± 88.8	438.9 ± 59.6	29.2	32.8
	Winter	RE	148.2 ± 25.5	130.5 ± 20.3	5.2	20.4
	Summer	GPP	528.8 ± 94.3	745.7 ± 91.2	3.1	3.3
	Winter	GPP	39.5 ± 5.8	37.5 ± 5.3	0.5	8.3
Paris	Summer	Total	2254.7 ± 539.9	2368.4 ± 136.3	403.6	74.8
	Winter	Total	5067.3 ± 1253.7	4924.4 ± 272.7	981.1	78.3
	Summer	Anthropogenic	2285.6 ± 538.7	2385.4 ± 131.6	407.1	75.6
	Winter	Anthropogenic	5033.1 ± 1253.7	4894.3 ± 272.5	981.2	78.3
	Summer	NEE	-30.9 ± 35.4	-17.0 ± 35.6	-0.2	-0.5
	Winter	NEE	34.2 ± 9.7	30.0 ± 9.2	0.5	5.1
	Summer	RE	133.4 ± 21.5	148.8 ± 21.7	-0.1	-0.6
	Winter	RE	51.7 ± 9.1	48.9 ± 8.5	0.6	6.7
	Summer	GPP	164.3 ± 28.1	165.8 ± 28.2	-0.1	-0.4
	Winter	GPP	17.4 ± 3.4	18.8 ± 3.6	-0.2	-6.0

References

Stagakis, S., Brunner, D., Li, J., Backman, L., Karvonen, A., Constantin, L., Järvi, L., Havu, M., Chen, J., Emberger, S., and Kulmala, L.: Intercomparison of biogenic CO_2 flux models in four urban parks in the city of Zurich, Biogeosciences, 22, 2133–2161, https://doi.org/10.5194/bg-22-2133-2025, 2025.